JCTC Journal of Chemical Theory and Computation

pubs.acs.org/JCTC Article

Plasmon Dynamics in Nanoclusters: Dephasing Revealed by Excited States Evaluation

Anant O. Bhasin, Yavuz S. Ceylan, Alva D. Dillon, Sajal Kumar Giri, George C. Schatz,* and Rebecca L. M. Gieseking

Cite This: J. Chem. Theory Comput. 2025, 21, 17−28 Read Online

ACCESS | Metrics & More | Article Recommendations | Supporting Information

ABSTRACT: The photocatalytic efficiency of materials such as graphene and noble metal nanoclusters depends on their plasmon lifetimes. Plasmon dephasing and decay in these materials is thought to occur on ultrafast time scales, ranging from a few femtoseconds to hundreds of femtoseconds and longer. Here we focus on understanding the dephasing and decay pathways of excited states in small lithium and silver clusters and in plasmonic states of the π-conjugated molecule anthracene, providing insights that are crucial for interpreting optical properties and photophysics. To do this, we study the time dependence of the electronic density matrix of these molecules using a new approach that expresses the density matrix in terms of TDDFT eigenstates (ESs) of the TDDFT Hamiltonian. This approach, which involves combining linear response time-dependent density functional theory (LR-TDDFT) and real-time time-dependent density functional theory (RT-TDDFT), leads to an analysis of the electron dynamics in terms of ESs, rather than individual molecular orbital (MO) transitions as has typically been done. This circumvents the complexities and subjective biases that traditional MO-based analysis provides. We find in an analysis of the induced dipole moment in these molecules that what had previously been considered to be energy relaxation is actually dephasing associated with the eigenstates that are stationary after the excitation pulse is turned off. We conclude that the ES-basis analysis has significant potential to advance understanding of the electron dynamics of plasmonic nanomaterials, aiding their optimization for photocatalytic and technological applications.

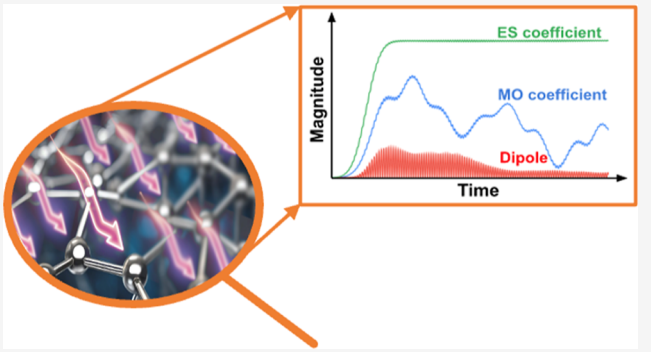

1. INTRODUCTION

Light-matter interactions in plasmonic nanomaterials, such as graphene and noble metal nanoparticles, induce a collective oscillation of the conduction electrons at specific frequencies, i.e., plasmon excitation, that is responsible for their characteristic vivid colors of the metal nanoparticles.[1−4] This phenomenon has enabled a wide range of applications, including in photovoltaics,[5−8] photocatalysis,[9,10] and surface enhanced Raman spectroscopy (SERS).[11−13] Although the plasmonic optical response is crucial for these applications, ultrafast nonradiative plasmon decay (on the scale of femtoseconds) limits the lifetimes of the energetic charge carriers (hot electrons and holes) and their utility.[7,14] This decay includes two distinct processes: electron−phonon scattering and electron−electron scattering. Understanding these decay mechanisms is essential to control or prolong plasmon lifetime, which is vital for optimizing their performance in various applications.

In contrast to nanoparticles, smaller nanoclusters (size < 1 nm) have more molecule-like spectra with electron−electron scattering as the dominant nonradiative decay pathway.[15−17] The significant dependence of this decay process on the physical and chemical attributes of the nanocluster has generated immense interest among theoretical and experimental chemists.[18−21] Results for thiolate-protected gold nanoclusters, Au_n (n = 36, 44, and 52), in face-centered cubic packing, suggest carrier lifetimes of ∼1−100 ns, which is significantly longer than the <1 ps lifetimes often considered for gold nanoparticles. This interest has been further enhanced by results for Au_{38} nanoclusters, in body-centered cubic packing, which exhibits a carrier lifetime of 4.7 μs, longer than that of semiconductor quantum dots and comparable to that of bulk silicon.[22] This illustrates the drastic changes in the decay properties of a nanocluster that are possible with a difference of only a few atoms.

Considering the immense phase space, experimental exploration of nanocluster dynamics is extremely demanding.

Received: October 1, 2024
Revised: December 16, 2024
Accepted: December 19, 2024
Published: December 31, 2024

In this regard, computational methods have much to offer. For example, linear response time-dependent density functional theory (LR-TDDFT) provides explicit excited states (eigenstates)[23−28] and has been used extensively to study the effect of shape and size in silver nanoclusters (Ag_n).[29−31] Recently, our group has shown that the frequency required to observe plasmon-like behavior increases with increasing width of Ag nanoclusters.[32] LR-TDDFT has also been useful in modeling highly conjugated organic molecules relevant to solar cell applications.[33] However, while facile for calculating absorption, LR-TDDFT provides no direct information about the electron dynamics underlying decay in these materials.

On the other hand, real-time time-dependent density functional theory (RT-TDDFT) provides an opportunity to capture the fast electron dynamics crucial for studying processes like nonradiative decay. Unlike LR-TDDFT, RT-TDDFT computes the system's response to a time-dependent electric field in the time domain.[34−36] This makes RT-TDDFT useful for studying electron dynamics in molecules and nanoparticles, including plasmon-like optical responses in noble metal linear chains and nanoclusters and their variation with environmental parameters.[33,37−39]

RT-TDDFT can be used in two ways: either as a complementary technique to LR-TDDFT in determining spectra or in providing crucial insights into electronic response at a specific frequency.[40−42] In the former mode, a δ-pulse of specific intensity is applied to generate excitations over a broad range of frequencies. Such real-time analysis has been used to assess the collective plasmon resonance in alkali and noble-metal linear atomic chains,[43,44] and to determine the correlation between linear nanowire length and dipole strength for different plasmonic excitations.[45] However, while performing such calculations it is essential to be cautious about the parameters of the applied electric pulse as application of higher intensity can produce a shift in the absorption peaks.[38] In the latter mode, a longer duration pulse at the plasmon frequency is used with results lending insight into electron dynamics and decay pathways. For example, Aikens et al.[46] analyzed an Ag_8 tetrahedral nanocluster in terms of its dipole response and variation of the molecular orbital (MO) occupancies and off-diagonal density matrix elements resulting from the interaction of the nanoclusters with a pulse. The changes in the occupation number revealed a plausible decay process characterized by a shift of density from one-photon to two-photon absorption states. Ma et al.[47] examined the evolution of a Ag_{55} icosahedral nanocluster with a similar method for analyzing fluctuations in the dipole moment and in MO-transition coefficients. Chapman et al.,[48] examined fullerene derivatives, providing theoretical evidence of plasmon decay leading to the generation of hot carriers. (Note: we use the term "fluctuation" to refer to time dependence where the peak amplitude in each cycle varies significantly with time, while "oscillation" is where the peak as essentially a constant.) In a study of naphthalene, Kuda-Singappulige et al.[49] coupled RT-TDDFT with Ehrenfest dynamics, to understand the role of nuclear motion in decay of a plasmon-like state.

LR- and RT-TDDFT offer different capabilities for understanding electronic processes in metal nanoclusters. LR-TDDFT can determine the true eigenstates (the excited states) of the system, but these eigenstates do not directly provide dynamical information regarding evolution of the electron density. On the other hand, RT-TDDFT allows us to track the evolution of MO occupation numbers in response to a pulse at a given frequency, which is crucial for understanding electron dynamics. However, since MOs are not the true eigenfunctions of the system, interpreting their evolution is challenging, which can obscure critical information about other decay pathways. For instance, Ma et al.,[47] while examining the evolution of the Ag_{55} nanocluster, analyzed transitions from occupied orbitals to only one virtual orbital (LUMO) and identified a decay pathway involving the generation of hot carriers. In contrast, another study on a similar system, Ag_{55}^{-3}, extended the analysis to include excitations to additional many virtual orbitals, uncovering a new plasmon decay pathway via two-photon states.[23] This demonstrates that the number of MOs considered in the analysis plays a crucial role in providing deeper insights into electron dynamics. However, interpretation of results in MO-basis is extremely cumbersome which can be seen from the variation of MO transitions coefficients for Ag_{55}^{-3} nanocluster. Furthermore, with the addition of each new atom, the number of possible MO transitions escalates dramatically, ultimately making the analysis based on MO-basis sets difficult to interpret.

Combining the advantages of the two approaches, we have developed a new methodology which captures electron dynamics in terms of excited states (ESs) instead of individual MO transitions. Our proposed methodology combines the electron dynamics from the RT-TDDFT with ESs from LR-TDDFT to provide clear interpretation of the results. This allows us to track the time evolution of the density matrix of the relevant LR-TDDFT ESs, avoiding the complications and significant fluctuations associated with traditional MO-basis analysis. While this approach does not go beyond the physical content associated with the TDDFT approximation and is still subject to self-interaction errors and basis set convergence issues, it does provide a much more precise description of the excited state dynamics than is available from an analysis of MOs for the clusters and molecule we are studying.

In this work, we utilize our methodology to analyze the optical response of lithium (Li_2) and silver (Ag_n, n = 2−8) metallic clusters, as well as the π-conjugated molecule anthracene. For the metal clusters transverse excitation with a pulse at the plasmon resonance energies leads to fluctuations in total dipole moment and MO-transition coefficients. These fluctuations are associated with dephasing of energetically nearby ESs that are excited within the energy bandwidth of the pulse excitation rather than their decay. The analysis shows that interference between different ESs correlates with fluctuations in the dipole moment, but the ESs themselves have constant coefficients with time after the pulse is over. Moreover, we explicitly observe independence of the ES dynamics with an increased density of states. Our study of anthracene is chosen to consider an organic molecule that is known to have plasmon-like ESs. In this case we are able to capture the constructive and destructive interference of individual MO-transitions in the magnitudes of the corresponding ES coefficients. This indicates the applicability of our approach to conjugated materials, such as graphene-based nanomaterials. Our methodology explicitly relates fluctuations in the dipole moment and MO-transitions to dephasing (a loss of coherence among ESs) rather than decay (a reduction in the population of any ES). Hence, our method clarifies the nature of the electronic response to an applied electric pulse and is applicable to a variety of systems.

https://doi.org/10.1021/acs.jctc.4c01302
J. Chem. Theory Comput. 2025, 21, 17−28

2. METHODOLOGY

2.1. Theory. Within LR-TDDFT, static calculations determine the ESs that represent poles in frequency-domain in response to an external time-dependent electric field. These ESs are linear combinations of multiple MO transitions. In the random-phase approximation (RPA), the transition density matrix operator, D_{0e}^{MO}, from the ground-state (GS) 0 to an excited-state (ES) e within a MO basis, is given by[50,51]

$$D_{0e}^{MO} = \sum_{mj} (X_{jm}^{0e} + Y_{jm}^{0e}) a_m^+ a_j \tag{1}$$

where X and Y are the coefficients for excitation and de-excitation, respectively, between occupied orbital j and unoccupied orbital m corresponding to excited state e. a_j and a_m^+ denote the creation and annihilation operators, respectively.

To relate the above static transition density matrix to the RT-TDDFT density matrix, it is crucial to understand the time dependence of the matrix elements. Considering that the eigenvalue equations to obtain ESs for LR-TDDFT and time-dependent Hartree−Fock (TDHF) are equivalent, the time-dependence of the matrix elements are analogous. Within TDHF, the calculation of ESs involves terms that provide the time dependence of the wave function[52]

$$C(t) = \sum_{mj} C_{mj} a_m^+ a_j = \sum_{mj} (X_{jm}^{0e} e^{-i\omega_\alpha t} + Y_{jm}^{0e} e^{+i\omega_\alpha t}) a_m^+ a_j \tag{2}$$

where $C(t)$ is the time dependent transition density matrix operator that evolves the system into a superposition of GS to ES, C_{mj} is the time-dependent coefficient of a particular excited state, ω_α is the excitation energy. Applying Euler's theorem we have

$$\begin{aligned} C(t) &= \sum_{mj} \varepsilon [X_{mj}(\alpha)(\cos(\omega_\alpha t) - i \sin(\omega_\alpha t)) \\ &\quad + Y_{mj}^*(\alpha)(\cos(\omega_\alpha t) + i \sin(\omega_\alpha t))] a_m^+ a_j \\ &= \sum_{mj} \varepsilon [\cos(\omega_\alpha t)(X_{mj}(\alpha) + Y_{mj}^*(\alpha)) \\ &\quad + i \sin(\omega_\alpha t)(-X_{mj}(\alpha) + Y_{mj}^*(\alpha))] a_m^+ a_j \end{aligned} \tag{3}$$

where, ε is a small numerical constant (determined by the excitation field) signifying the amplitude of fluctuations or small perturbations in the system.

In RT-TDDFT, the system's response to a time-dependent electric field is evaluated in the time domain by evolving the density matrix over time. This evolution is computed in terms of the atomic orbital basis set, which can be readily converted to the MO basis set as[50]

$$D^{MO}(t) = z^\dagger D^{AO}(t) z \tag{4}$$

where, z is the LCAO-MO coefficient matrix.

In the evolution of the system, the time-dependent wave function is formally defined through the exponential expansion[52]

$$|\Psi(t)\rangle = \exp[C(t)]|\Psi_0(t)\rangle \tag{5}$$

where $|\Psi_0(t)\rangle$ and $|\Psi(t)\rangle$ represent the wave function of the GS and the final wave function of the evolved system, respectively.

When applying a small perturbation to the system, we can expand the exponential in eq 5 and truncate in first order.

$$|\Psi(t)\rangle = (1 + C(t))|\Psi_0(t)\rangle = |\Psi_0(t)\rangle + \sum c_e(t)|\Psi_e(t)\rangle \tag{6}$$

where $c_e(t)$ and $|\Psi_e(t)\rangle$ represent the coefficient and wave function, respectively, of an ES. This evolution, assuming small c_e, results in a superposition of the GS and ESs, with the density matrix

$$\begin{aligned} \rho_{\Psi(t)} &= |\Psi(t)\rangle\langle\Psi(t)| \\ &\approx |\Psi_0(t)\rangle\langle\Psi_0(t)| + \sum c_e^*(t)|\Psi_0(t)\rangle\langle\Psi_e(t)| + \\ &\quad \sum c_e(t)|\Psi_e(t)\rangle\langle\Psi_0(t)| \\ &\approx D_0^{MO} + \sum c_e^*(t) D_{0e}^{MO\dagger} + \sum c_e(t) D_{0e}^{MO} \end{aligned} \tag{7}$$

Therefore, the system can exist in a pure ES or a superposition of multiple ESs, evolving in terms of $(X + Y)$ for real elements and $(-X + Y)$ for imaginary elements, as specified in eq 3. This involves a linear combination of the transition density matrices of corresponding excited states. The actual real-time density matrix in RT-TDDFT can be projected onto each excited state. Using these matrices, we calculate the coefficient of i-th ES using the density matrix linear response MOs ($P_{MO,LR}$) as

$$\mathrm{Re}(P_{ES(i)}) = \mathrm{Re}(P_{MO,LR}^{-1}) : (X_i + Y_i) \tag{8a}$$

$$\mathrm{Im}(P_{ES(i)}) = \mathrm{Im}(P_{MO,LR}^{-1}) : (-X_i + Y_i) \tag{8b}$$

where the colon indicates a double dot product (multiplying the two matrices element by element, and then summing all products).

2.2. Simulation Details. All geometries were optimized using density functional theory (DFT) with random phase approximation (RPA) and PBE functional.[53,54] For silver nanowires, we utilized the cc-pVDZ-PP (pseudopotential) correlation-consistent valence-only basis set.[55] For Li_2 and the anthracene molecule, the cc-pVDZ basis set (without pseudopotential) was employed. The same functional and basis sets were used for LR-TDDFT and RT-TDDFT simulations.[56,57] In LR-TDDFT simulations, we computed 150 static excited states for Li_2 and 200 for all the silver nanowires and anthracene. The spectra obtained from LR-TDDFT were subjected to Lorentzian broadening with a factor of 0.12 eV for better visualization. The PBE functional has often been used for describing plasmonic excitations in silver and gold clusters, and in many computational applications, optical spectra obtained from TDDFT calculations with PBE and other GGA functionals in combination with pVDZ basis sets have been found to be in good agreement with higher quality calculations,[58] in part because the transitions involved in plasmon excitations are very much dominated by free-electron states. In addition, transitions related to band gap excitations are not important for metallic systems.

Given our focus on electron dynamics, we kept the nuclei fixed, thereby preventing energy dissipation through electron−phonon coupling and restricting energy transfer to that between ESs. In RT-TDDFT simulations, electric pulses were applied at a peak intensity of 0.0001 au, unless stated otherwise. The density matrix evolved over time in response to the applied pulse, starting from the ground state density matrix.

https://doi.org/10.1021/acs.jctc.4c01302
J. Chem. Theory Comput. 2025, 21, 17−28

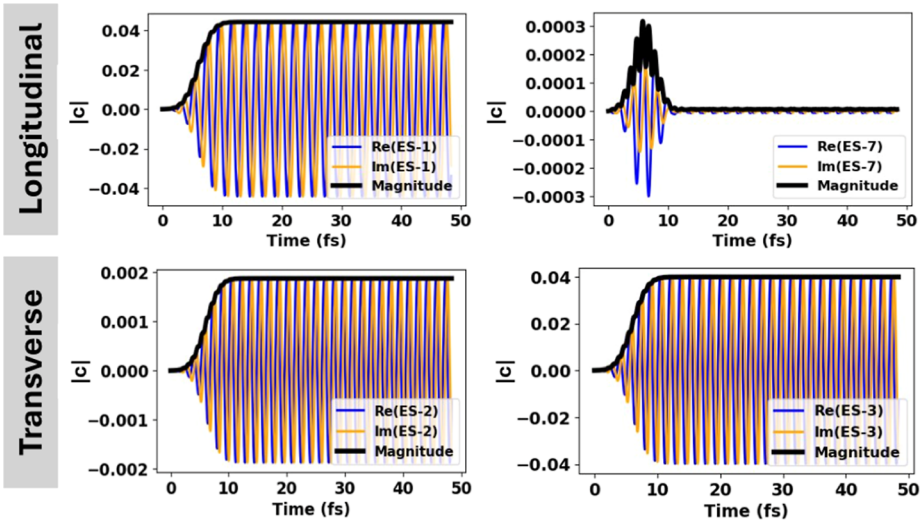

Figure 1. Evolution of ES coefficients, c, for Li_2 subjected to a 1.97 eV longitudinal electric pulse (top) and a 2.58 eV transverse electric pulse (bottom). Excited states in the range of c_{max} to $c_{max}/1000$ are shown here, with the most important transition on the left for 1.97 eV and on the right for 2.58 eV.

Each simulation used a time step of ∼0.0048 fs (0.2 au) and was terminated at 48.37 fs (2000 au), unless stated otherwise. For the RT-TDDFT simulation with a δ-pulse, the absorption spectra were obtained by performing a Fourier transform of the induced dipole oscillations. The frequency of all pulses was set equal to the most intense absorption peak calculated from the RT-TDDFT δ-pulse. To study the systems' evolution, a Gaussian envelope pulse with a width of 1.94 fs was centered at 6 fs. All simulations, including geometry optimization, LR-TDDFT, and RT-TDDFT, were conducted using NWChem software version 7.0.0.[59]

3. RESULTS AND DISCUSSION

3.1. Li_2—A Prototypical System. Alkali metals are recognized for their ability to support plasmons and have been extensively studied.[42,60] They also have a single electron in their valence shell, like Ag and Au. Because Li_2 is a small molecule, it is not expected to exhibit plasmonic behavior. Rather, we used it to establish our approach and evaluate the accuracy of our analysis. A detailed pedagogical explanation, including a deeper exploration of these concepts, is provided in the Supporting Information.

We calculated absorption spectra for Li_2 in both the frequency and time domains using LR-TDDFT and RT-TDDFT, respectively. In order to consistently combine the two approaches, it is essential that they produce nearly identical absorption spectra. As shown in Figure S1a, consistent resonances were found at 1.97 eV (ES 1) for longitudinal (z polarized) pulses and at 2.58 eV (degenerate ES 2 and ES 3) for transverse (x/y polarized) pulses.

Next, we explored the electronic response of Li_2 under Gaussian pulses at resonant frequencies using the RT-TDDFT calculations. Li_2 has a sparse state density for excitation in the few eV range, so we would expect that resonant excitation would lead to a single excited state after the pulse that does not decay in time. Indeed, longitudinal excitation with a pulse at 1.97 eV (resonant with ES 1) resulted in an increased dipole moment during the pulse interaction time, and with the amplitude remaining constant afterward as shown in Figure S2. Also, the HOMO → LUMO transition dominates the excitation, with the next most important transitions, HOMO → LUMO + 6, and HOMO → LUMO + 16, having smaller coefficients by an order of magnitude (Figure S3). The results for excitation along the transverse (x) axis with a pulse at 2.58 eV (resonant with ES 3) produced similar behavior (Figure S4), with HOMO → LUMO + 1 being the most important transition, and HOMO → LUMO + 2, and HOMO → LUMO + 8, being lower by an order of magnitude (Figure S5). Transformation of these results into the LR-TDDFT excited state basis confirmed that the system's response involved stationary excited states, primarily ES 1 for longitudinal excitation and primarily ES 3 for transverse excitation (Figure 1). A detailed explanation is provided in the Supporting Information.

3.2. Ag Nanowires. Silver nanowires have been studied in the past as model systems for electronic excitations, including the structural dependence of dipole strengths and excitation energies.[27,40,61−65] Although these effects have not been realized experimentally, they provide valuable insights into the ES dynamics in ligand-protected silver nanoclusters which are well-established. In this study, we systematically analyze silver nanowires with varying numbers of silver atoms (Ag_n, n = 2, 4, 6, and 8). The LR-TDDFT absorption spectra match those obtained in previous studies[62,63] (see Figure S6). As the nanowire length increases, the longitudinal peak's energy decreases and intensity increases, while the transverse peak hardly changed.

3.2.1. Ag_2. Similar to Li_2, we examined the agreement between LR-TDDFT and RT-TDDFT results with a δ-pulse for the Ag_2 nanowires. The spectral features from the two methodologies align with a precision of ∼0.02 eV for Ag_2 nanowire as shown in Figure 2. The absorption spectrum highlights three distinct peaks: one along the z-axis (longitudinal) with an energy of 3.09 eV and two along the x/y-axis (transverse) with energies of 4.44 and 4.74 eV. The transverse peaks exhibit significantly different absorption intensities corresponding to differences in their transverse dipole moment (Table S2). To incorporate for the effect of field applied along the y-axis which gives identical response to the x-axis, we doubled the intensity of the x-axis response. As determined by LR-TDDFT, the energies of these peaks

https://doi.org/10.1021/acs.jctc.4c01302
J. Chem. Theory Comput. 2025, 21, 17−28

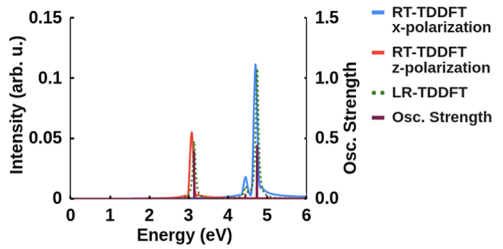

Figure 2. Absorption spectra for Ag_2 calculated from LR-TDDFT and RT-TDDFT using a δ-pulse.

correspond to the ES 1, with a dipole moment along the z-axis, and degenerate pairs ESs 3, 4 and 5, 6 with dipole moments along the x, y-axes. Based on the transition dipole moment magnitudes, we selected ES 1 and ES 6 for resonant excitation to induce electron dynamics.

The left side of Figure 3 shows the results of a RT-TDDFT simulation with a longitudinal Gaussian pulse with excitation energy resonant with ES 1, polarized along the z-axis leading to longitudinal excitation. The field amplitude decays to nearly zero by 12 fs, and the simulation ran until approximately 50 fs. The induced dipole moment increases during interaction with the pulse, and then oscillates with a constant amplitude when the interaction is over. By analyzing the transition matrices from RT-TDDFT, we identified four MO transitions that significantly contribute to ES 1, with the HOMO → LUMO transition exhibiting highest intensity, which is in agreement with LR-TDDFT (Table S2). We focus on the magnitude of these four MO transition coefficients, omitting the individual real and imaginary components, Figure 2 (center). The significant oscillation (oscillate between constant maxima and minima) in the magnitude of these MO transitions highlights the complexity of the analysis using the MO-basis. On the other hand, analysis in the ES-basis reveals that the coefficient of ES 1 first increases and then is constant after the pulse is over. Given the dominance of the HOMO → LUMO transition, we expect the evolution of ES 1 to be primarily governed by the evolution of this MO transition coefficient. Similar to the longitudinal ES evolution observed in Li_2 we anticipated no change in the coefficient of ES 1 with time after interaction with the pulse ends. The consistent evolution of the MO transition and ES 1 suggests a strong agreement with our analysis scheme (Table S2). We expect the system to remain in a superposition of GS and ES 1.

The bottom of Figure 3 shows the results of a RT-TDDFT simulation with a Gaussian pulse having a central frequency resonant with ES 6 and transverse polarization. In this case, the dipole moment displayed periodic fluctuations (changes in magnitude of maxima and minima). Transitioning from Li_2 to Ag_2, entailing a larger number of electrons, LR revealed a distinctive feature in the transverse states. In contrast to the longitudinal excitation, there is not one dominant MO transition. The main absorption mode is composed of six transitions with significant amplitude. In RT-TDDFT, the six distinct MO transitions show large coefficients, with substantial fluctuations that maintain a phase relation. For example, the transition HOMO → LUMO + 1, with the highest coefficient, exhibits variations in harmony with the HOMO − 3 → LUMO transition, and a similar behavior can be seen for HOMO − 9 → LUMO + 3, and HOMO − 2 → LUMO. These repeated fluctuations are typical for an interference pattern that involves strongly interacting single particle transitions.

Analysis in the ES basis shows that, in contrast to the cases described previously, ESs 4 and 6 both have significant magnitudes that are constant after the pulse is turned off. Although the central laser energy is resonant with only one ES, its inherent width causes it to overlap with the energies of nearby states. The energy-time uncertainty principle dictates that a pulse with a precise energy (narrow energy width) would require an infinitely long duration, as in case with a CW laser. However, a pulse of finite duration inevitably possesses a certain energy width, leading to the excitation of nearby ESs.

Interference between the ESs 4 and 6 is highly probable as both ESs exhibit significant dipole moments along the x-axis. (Note that the states ESs 3 and 5, that are degenerate with ESs 4 and 6, respectively, are y-polarized and thus do not contribute.) To further elucidate this behavior (Figure 4), we compared the dipole moment fluctuations with the expected time scale derived from the 0.292 eV energy difference between the two ESs. The corresponding frequency is approximately 7.19×10^{13} Hz, giving a period of around 13.9

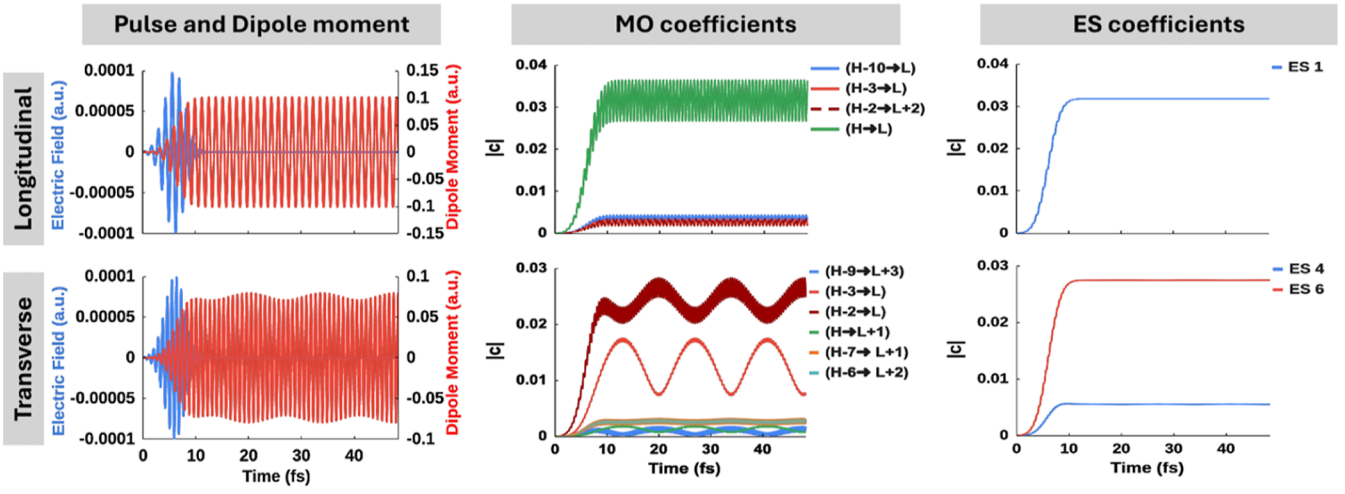

Figure 3. Response of Ag_2 to a Gaussian pulse (top) longitudinal excitation at 3.14 eV and (bottom) transverse excitation at 4.74 eV. (Left) Applied field and resulting dipole moment, (center) MO transition coefficients, and (right) ES-coefficients in the range of c_{max} to $c_{max}/10$ (bottom). Here, H = HOMO and L = LUMO.

https://doi.org/10.1021/acs.jctc.4c01302
J. Chem. Theory Comput. 2025, 21, 17−28

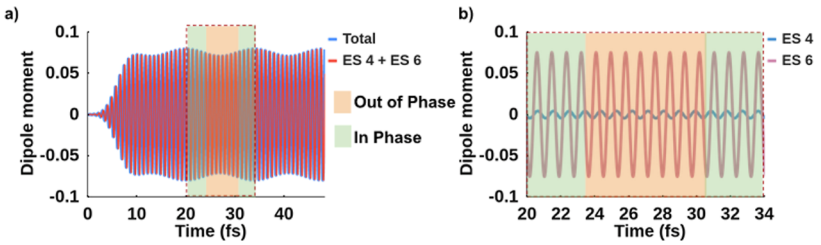

Figure 4. (a) Total dipole moment along the *x*-axis and the contribution of ES 4 + ES 6. (b) Separate dipole moment contributions from ES 4 and ES 6, initially in-phase, fully out-of-phase at ∼27 fs, and in-phase again at 34 fs.

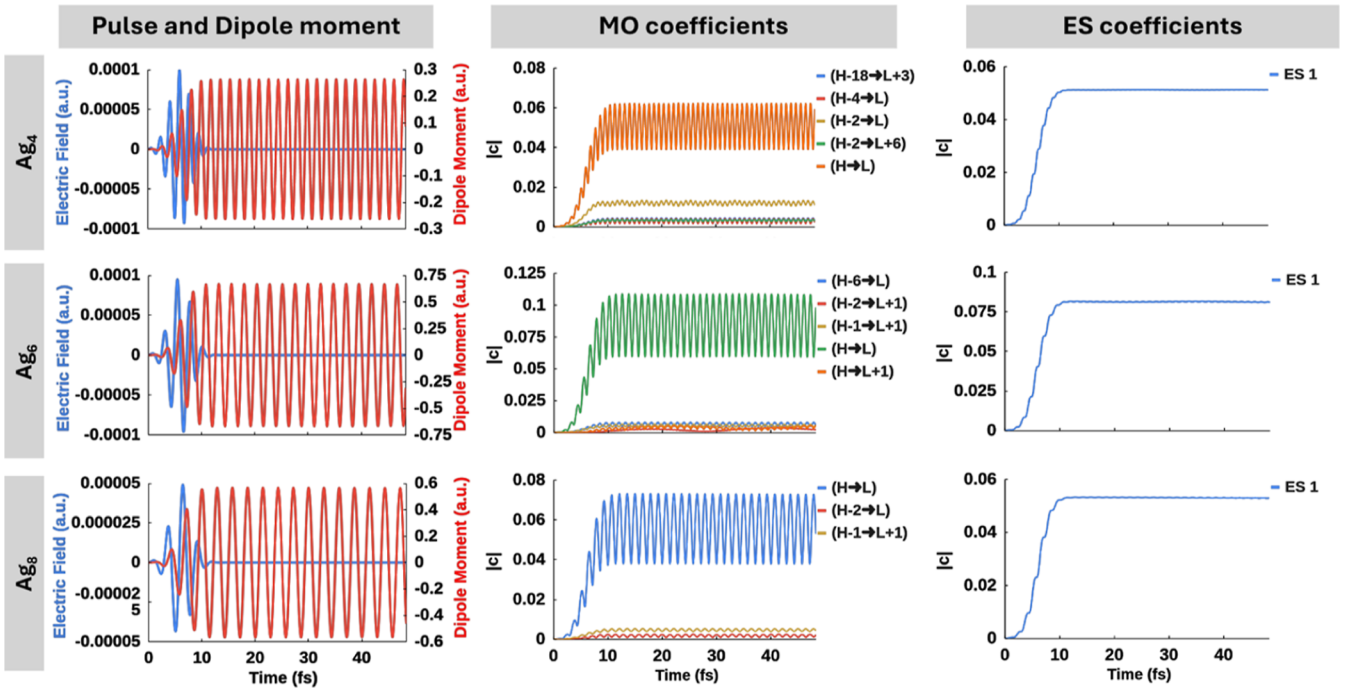

Figure 5. (Left) Applied longitudinal electric field and dipole response, (center) MO transition coefficients, and (right) ES-coefficients for Ag_4 (top), Ag_6 (middle) and Ag_8 (bottom). Here, H = HOMO, L = LUMO and ES = excited state.

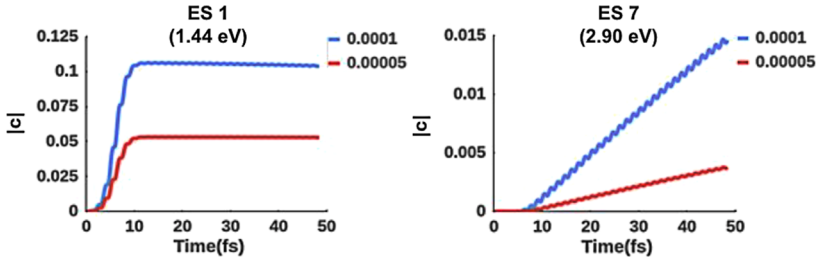

Figure 6. Coefficient of ES 1 (left) and ES 7 (right) for a Ag_8 nanowire subjected to electric field intensities of 0.0001 (blue) and 0.00005 atomic units (red).

fs, which closely matches the calculated period (13.956 fs). This confirms that the energy difference and resulting phase interference are responsible for the observed fluctuations.

Overall, results in the ES-basis are more transparent and insightful than those in the MO basis. The analysis reveals both the excitation of individual ESs and the interference between energetically nearby states. The fluctuations of the dipole moment were explicitly related to specific ESs, with the interference between these states being more evident in the ES-basis than in the MO-basis.

3.2.2. $Ag_{4/6/8}$. We conducted a comprehensive analysis of Ag_4, Ag_6, and Ag_8 nanowires to understand their electronic responses to applied electric pulses using LR-TDDFT and RT-TDDFT. Again, LR-TDDFT provided ESs with MO transitions and their coefficients (Tables S3−S5). For all the nanowires, spectra provided by LR-TDDFT (Figure S6) and RT-TDDFT were in good agreement. It is noteworthy that the energy of ES 1 decreased with increasing length of the nanowire, as might be expected for a particle in box problem.

We performed RT-TDDFT with Gaussian pulses and frequencies resonant with the most intense peaks along longitudinal and transverse ESs and analyzed the dipole response to the applied electric field, the MO transitions, and ESs for deeper insights into these systems. The results for

https://doi.org/10.1021/acs.jctc.4c01302
J. Chem. Theory Comput. 2025, 21, 17−28

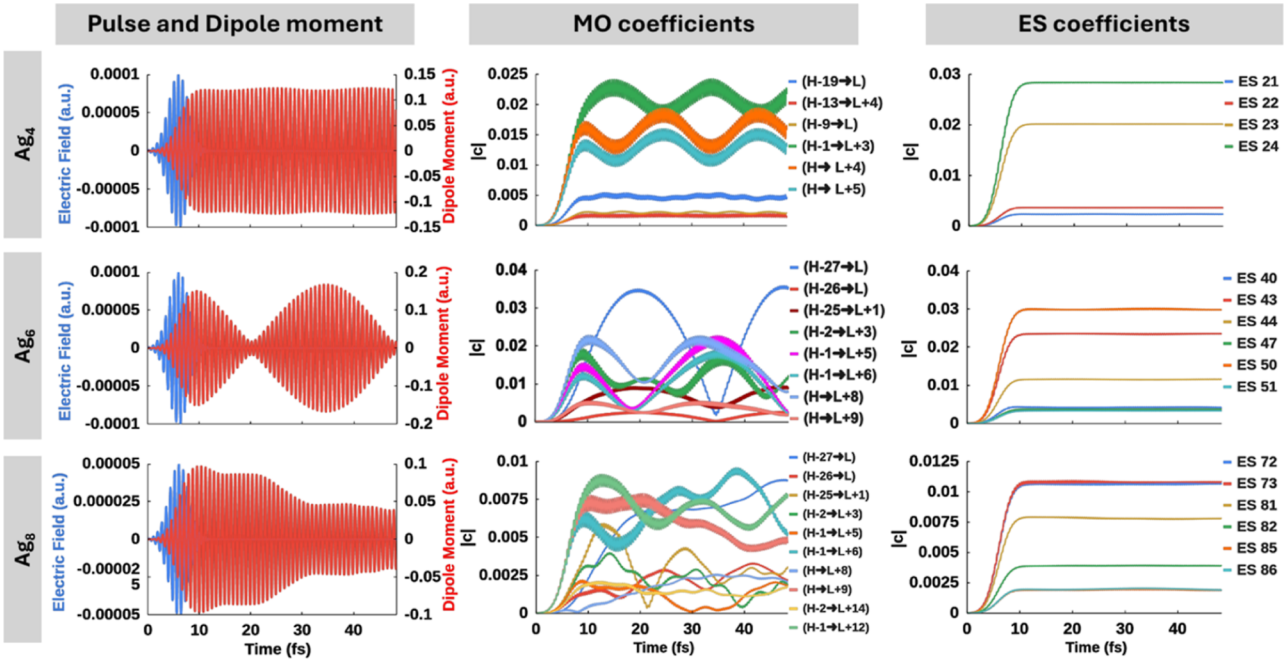

Figure 7. (Left) Applied transverse electric field and dipole response, (center) MO transition coefficients, and (right) ES-coefficients for Ag_4 (top), Ag_6 (middle) and Ag_8 (bottom). Here, H = HOMO, L = LUMO and ES = excited state. Evolution of all Ag_8 ESs are provided in Supporting Information (Figure S10).

longitudinal pulses are shown in Figure 5. For all the nanowires longitudinal pulses at a frequency resonant with ES 1 produced a similar pattern in the dipole moment: after an initial increase, the magnitude remained constant. In the MO analysis, the HOMO → LUMO transition was the most prominent, with small coefficients for multiple other MO-transitions. As expected, ES analysis showed no fluctuations in the ES 1 coefficient for all the nanowires. Similar to previous case, the system remains in a superposition of GS and ES 1 for the longitudinal excitation. Thus, for the main longitudinal absorption peak, results from the MO-basis and ES-basis analyses are in agreement.

In Ag_8, we observed an additional interesting phenomenon: with a sufficiently strong electric field, two distinct ESs (ESs 1 and 7) gained significant intensity (Figure 6). The energy of ES 7 (2.90 eV) was found to be approximately twice that of ES 1 (1.44 eV), suggesting that ES 7 might be a two-photon excitation. This response is similar to that observed by Aikens et al. for the Ag_8 tetrahedral cluster.[46] Since the Ag_8 wire has a center of symmetry, one-photon and two-photon excitations are mutually exclusive. Additionally, ES 7 has zero transition moment along the z-axis, further supporting our hypothesis of a two-photon excitation. To test this possibility, we decreased the intensity of the electric field and observed the coefficients of the ESs. While linear absorption is proportional to the light intensity, two-photon absorption is proportional to the square of the light intensity. By decreasing the pulse intensity to half, we observed that the coefficient of ES 1 was reduced to half and the coefficient of ES 7 was reduced to a quarter of their original values, confirming that ES 7 is populated via two-photon excitation. Hence, to be consistent for Ag_8 along both the longitudinal and transverse axes, we applied an electric pulse of intensity 0.00005 au Small fluctuations in the ESs are numerical issues while calculating real and imaginary coefficient in RT-TDDFT without any physical significance.

Figure 7 shows our results for transverse excitation of the Ag nanowires. For Ag_4, we applied a pulse corresponding to ES 24 (4.99 eV). The dipole moment displayed very minor periodic fluctuations in response to the applied electric field. Four MO transitions were significant (HOMO − 1 → LUMO + 3, HOMO → LUMO + 4, and HOMO → LUMO + 5), exhibiting large coefficients (Table S3). Similar to the result of Ag_2 transverse excitation, we observed huge fluctuations in sync with each other. In contrast, the four ESs[21−24] with significant coefficients exhibited no fluctuations, after their initial increase. Among them, ESs 21 and 22 are degenerate, as are ESs 23 and 24. Similar to Ag_2, these minor dipole moment fluctuations were found to be due to interference between these four ESs which are very close in energy (Figure S7).

In contrast to Ag_4, the Ag_6 nanowire showed very large periodic fluctuations in the total dipole moment in response to an applied transverse Gaussian pulse resonant to ES 50. The sustained periodicity of these fluctuations was validated by extending the simulation time to ∼85 fs (Figure S8). MO analysis showed seven distinct MO transitions with notable coefficients exhibiting substantial fluctuations, some of which appear synchronized (Table S4). Notably, the peaks of the HOMO − 27 → LUMO transition align precisely with the troughs of HOMO − 1 → LUMO + 5, HOMO − 1 → LUMO + 6, and HOMO → LUMO + 8 transitions. Additionally, excitations from MOs well below the HOMO exhibit substantial coefficients. In other words, we observe the presence of interband (d → sp) transitions. To understand this excitation in terms of ESs, we noted significant coefficients for six distinct ESs,[23,40,43,44,47,50] including two degenerate pairs (ESs 43, 44 and ESs 50, 51). That ESs 43 and 50 have notably higher coefficients than their degenerate partners is due to significantly larger transition dipole moments along the x-axis (Table S4). The other two ESs (ESs 40 and 47) showed small populations and transition moments compared to the degenerate ESs. Hence, the two degenerate pairs of ESs with

https://doi.org/10.1021/acs.jctc.4c01302
J. Chem. Theory Comput. 2025, 21, 17−28

high coefficients dictate most of the dipole response of the system, providing a similar response to Ag_2 and Ag_4. This observation implies that the system persists in a superposition of multiple excited states throughout the simulation. The dipole moment contributions from all the ESs with substantial coefficients (ESs 43, 44 and 50) exhibit interference pattern similar to the total dipole moment (Figure S7).

For Ag_8, we applied a transverse Gaussian pulse with a frequency resonant with ES 72 (4.97 eV) corresponding to the largest dipole moment (3.814 D). Instead of periodic fluctuations throughout the simulation, we observe significant damping of the total dipole moment over time. In terms of MO transitions, we observed more transitions with significant coefficients (Table S5). These coefficients vary with time and some transitions are in phase with one another. However, the significant fluctuations of the MO transitions with no obvious repeating pattern, depict energy being redistributed among states in complicated ways. Analyzing in the ES basis, we observed 12 different ESs gaining significant excitation (Table 1, six are omitted from Figure 7 for clarity). Interestingly, we observed no significant fluctuations in the coefficients of these ESs. The application of a Gaussian pulse excited the system to these ESs (Table 1) and their interference resulted in the damping of the dipole seen in the MO basis. Thus, the complexities observed in the MO basis are artifacts, highlighting the usefulness of the ES basis.

Table 1. Excited State Analysis in Terms of Frequency and Dipole Moment for Ag_8 Transverse States[a]

degenerate excited states	dipole moment along x-axis (D)	frequency (10^{15} Hz)	energy (eV)
61,62	1.73, 1.66	1.15	4.74
<u>72,73</u>	<u>−3.81, 3.81</u>	<u>1.20</u>	<u>4.97</u>
74,75	2.61, 2.57	1.20	4.98
77,78	−2.36, 2.40	1.21	5.02
81,82	−2.89, −1.43	1.22	5.04
85,86	−0.74, −0.76	1.23	5.10

[a]The states that are resonant with the applied Gaussian pulse are underscored.

Utilizing our analysis in the ES basis, we successfully captured and modeled the dephasing between various ESs and identified specific ESs whose interference induces fluctuations in the total dipole moment. Although MO transitions exhibit intriguing patterns, even a small system like Ag_8 presents a large number of MO transitions with substantial coefficients. All these coefficients display huge fluctuations and analyzing these transitions is not only tedious but also prone to misinterpretation. In contrast, examining the evolution in the appropriate basis clearly reveals the essential dephasing of various excited states. Our approach offers a more rigorous, clean, and efficient analysis of the electron dynamics.

3.3. Anthracene. To evaluate the effective range of our analysis, we expanded our investigation to anthracene, an organic molecule known for its plasmon-like β-peak.[49] Figure 8 shows the anthracene absorption spectrum. The β-peak is created by the constructive interference of two MO transitions, namely HOMO − 1 → LUMO and HOMO → LUMO + 1. Constructive interference between these transitions leads to a significant transition dipole moment (−3.89 D), which is characteristic of a plasmonic excitation. In contrast, the α-peak, arises due to destructive interference between the same MO transitions, resulting in cancellation of the transition dipole moments (−0.08 D) and failure to produce a plasmonic response. The key point is that the β-peak corresponds to a strong transition dipole moment, which is why it is identified as plasmon-like, while the α-peak does not exhibit that behavior. Here we present results for the longitudinally excited α- and β-peaks (at 3.97 and 5.35 eV, respectively), while the Supporting Information shows results for one of the transverse excited p-peaks.

Figure 9 shows the electronic response of anthracene to applied longitudinal Gaussian pulses with RT-TDDFT. For the Gaussian pulse with frequency resonant to the β-peak, we observe no variation in the amplitude of the dipole oscillations after the pulse is turned off. In the MO-basis, HOMO − 1 → LUMO and HOMO → LUMO + 1 gained significant coefficients and were the major contributors for the β-peak. The coefficients of these MO-transitions were large, resulting in strong absorption. In the ES-basis, we observe a high coefficient for ES 5 corresponding to the β-peak with no fluctuations.

For the Gaussian pulse with frequency resonant to the α-peak, we observed that the dipole moment closely mirrored the behavior of the applied pulse, increasing and decreasing in sync with the pulse's oscillations. The decrease in dipole moment between 6 to 12 fs is due to partially exciting the β-peak while the pulse is on. However, as the β-peak is too far from resonance, it cannot sustain any population. In the MO basis, we observed the excitation of the same two MO transitions; however, their coefficients were significantly smaller than for the β-peak due to destructive interference between them. Once the pulse was turned off, the MO coefficients leveled off. In ES-basis, we observe that after the pulse is over, the α-peak (ES 2) is mainly excited. As expected, we observe no fluctuations in the ES coefficients, consistent with the dipole response and MO transitions. The initial, transient excitation into ES 5 is

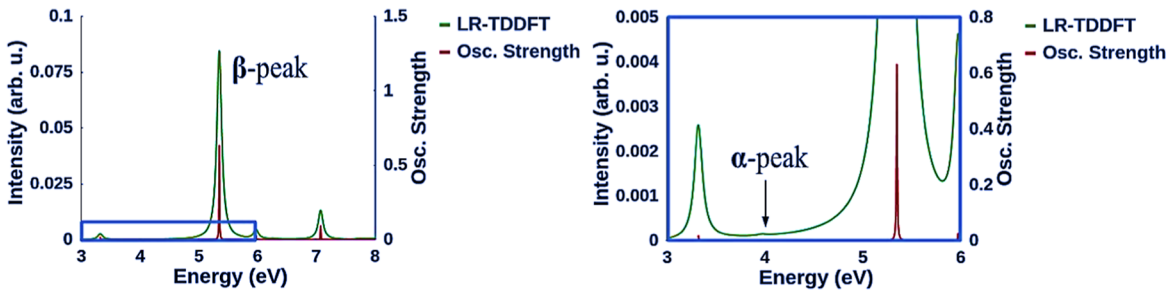

Figure 8. Absorption spectrum of anthracene molecule from LR-TDDFT at PBE/cc-pVDZ level of theory: the full spectrum (left) shows the β-peak at 5.35 eV and the detail (right) locates the relatively weak α-peak at 3.97 eV.

https://doi.org/10.1021/acs.jctc.4c01302
J. Chem. Theory Comput. 2025, 21, 17−28

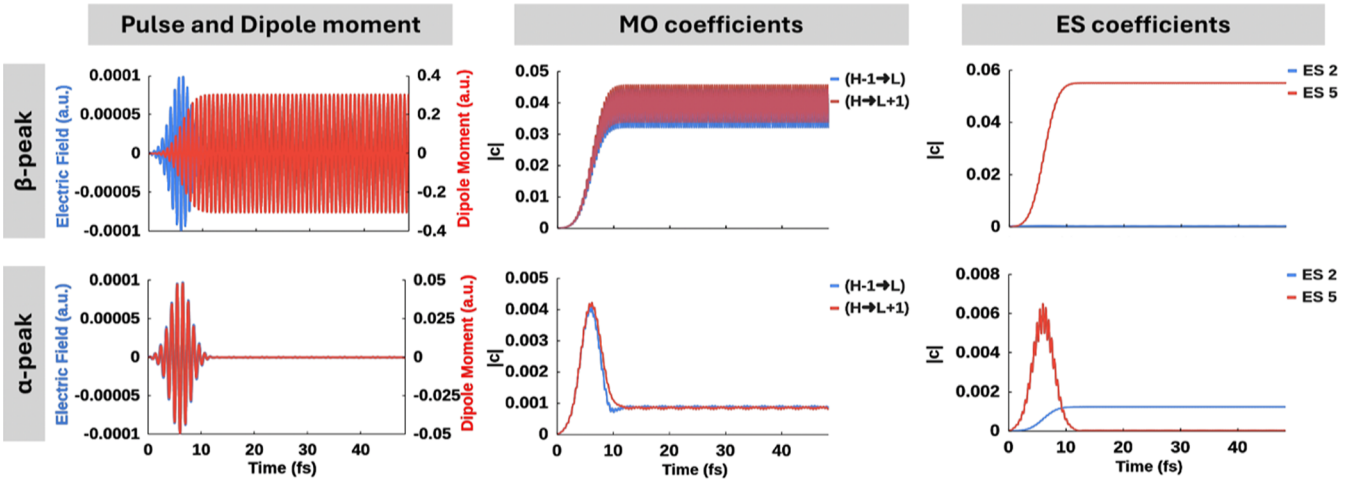

Figure 9. Results for anthracene's β-peak (top) and α-peak (bottom), including the longitudinally applied electric field and dipole response (left), corresponding MO transitions (center) and ES-analysis (right). H = HOMO, L = LUMO and ES = excited state.

strong only because the dipole moment for ES 5 is much larger than for ES 2.

Overall, this analysis depicts the usefulness of applying our ES-basis analysis to absorption by an organic molecule. Our analysis provides a clearer and more concise description of the electronic response of an acene, capturing the interference of MO transitions in terms of the simpler evolution of the ES coefficients.

4. CONCLUSION

Plasmonic nanoclusters exhibit efficient photocatalytic efficiency. However, limitations in the understanding of electron dynamics under applied electric fields poses a significant obstacle to their practical application. To address this challenge, we developed a novel methodology that analyzes the density evolution in terms of ESs instead of the conventional approach based on an MO-basis. In this study, we employed RT-TDDFT and LR-TDDFT techniques to investigate the plasmon-like characteristics of both metallic nanowires and an acene. In both cases the ES-based analysis offers a more realistic and mechanistic description than the commonly used MO version. The applied pulse can result in one of the following:[1] excitation into a specific ES, where the magnitude of the overall dipole moment remains constant. For instance, longitudinal excitation of all the nanowires shows this.[2] Excitation into primarily two ESs with fluctuations in the magnitude of the overall dipole moment. Transverse excitation of diatomic clusters with low state densities, such as Li_2 and Ag_2, shows this most clearly.[3] Excitation into many ESs with fluctuations in the overall dipole moment. For instance, we found this for transverse excitation of large silver nanowires. Moreover, what we learn from this analysis is that the time dependence of the dipole moment on the relevant time scales is entirely governed by dephasing between what are otherwise stationary ESs after the pulse is over. In the larger silver nanowires, we encountered substantial fluctuations in the dipole moment due to interference between multiple ESs with significant coefficients. This is especially important to the analysis of Ag_8 nanowires, where the MO dipole moment shows nonperiodic evolution, marked by a significant decrease over time. Here we found that what might be considered a damping phenomenon was readily explicable through interference effects among ESs with large coefficients. We applied a pulse with 2 fs width which excited a broad distribution of eigenstates, and this makes dephasing occur on a very short time scale (~2 fs) while the pulse is being turned off. Expanding our analytical framework to encompass organic molecules with plasmon-like states also yielded valuable insights, in this case showing that highly off-resonant states with high transition moments can be important during the pulse but then disappear after the pulse is over. We anticipate that extending this analysis to graphene-based nanomaterials could offer further elucidation of energy flow in such systems. Further, the stationary behavior found for the electronic states of clusters studied in this work is consistent with the measured long lifetimes of the Au clusters (~100 ns) mentioned in the Introduction. Adding nuclear motion into the dynamics is not expected to change this picture unless the spacing between electronic energy levels is reduced (by adding more atoms to the cluster) to values comparable with the vibrational quanta. Overall, the present analysis serves as an important starting point to future studies where we consider the effect of dynamics beyond that contained in the TD-DFT description of the electronic states.

■ ASSOCIATED CONTENT

Supporting Information

The Supporting Information is available free of charge at https://pubs.acs.org/doi/10.1021/acs.jctc.4c01302.

This document is organized into three sections. Section A presents the response of Li_2 to Gaussian pulses applied along the longitudinal and transverse axes. Section B discusses the absorption spectra of various silver nanowires, comparing their maximum absorption peaks. It also includes the response of these nanowires to an applied longitudinal pulse, along with tables detailing the ESs and the contributions of multiple MOs to specific ESs. Section C explores the response of anthracene to an out-of-plane Gaussian pulse (p-peak) (PDF)

■ AUTHOR INFORMATION

Corresponding Author

George C. Schatz − *Department of Chemistry, Northwestern University, Evanston, Illinois 60208, United States;*

https://doi.org/10.1021/acs.jctc.4c01302
J. Chem. Theory Comput. 2025, 21, 17−28

orcid.org/0000-0001-5837-4740; Email: g-schatz@northwestern.edu

Authors

Anant O. Bhasin − *Department of Chemistry, Brandeis University, Waltham, Massachusetts 02453, United States;* orcid.org/0009-0000-8042-7466

Yavuz S. Ceylan − *Department of Chemistry, Brandeis University, Waltham, Massachusetts 02453, United States; Department of Chemistry, Massachusetts College of Liberal Arts, North Adams, Massachusetts 01247, United States*

Alva D. Dillon − *Department of Chemistry, Brandeis University, Waltham, Massachusetts 02453, United States*

Sajal Kumar Giri − *Department of Chemistry, Northwestern University, Evanston, Illinois 60208, United States;* orcid.org/0000-0001-9145-6801

Rebecca L. M. Gieseking − *Department of Chemistry, Brandeis University, Waltham, Massachusetts 02453, United States;* orcid.org/0000-0002-7343-1253

Complete contact information is available at: https://pubs.acs.org/10.1021/acs.jctc.4c01302

Notes

The authors declare no competing financial interest.

■ ACKNOWLEDGMENTS

A.O.B. and R.L.M.G. acknowledges the NSF grant CHE-2046099. Computational work was performed on the Brandeis HPCC, which is partially supported by the NSF through DMR-MRSEC 2011846 and OAC-1920147. S.K.G. and G.C.S. acknowledge NSF grant CHE-2347622. We thank Prof. Judith Herzfeld for helpful discussions and feedback on manuscript.

■ REFERENCES

(1) Matus, M. F.; Häkkinen, H. Understanding Ligand-Protected Noble Metal Nanoclusters at Work. *Nat. Rev. Mater.* **2023**, *8* (6), 372−389.

(2) Schuller, J. A.; Barnard, E. S.; Cai, W.; Jun, Y. C.; White, J. S.; Brongersma, M. L. Plasmonics for Extreme Light Concentration and Manipulation. *Nat. Mater.* **2010**, *9* (3), 193−204.

(3) Koppens, F. H. L.; Chang, D. E.; García de Abajo, F. J. Graphene Plasmonics: A Platform for Strong Light−Matter Interactions. *Nano Lett.* **2011**, *11* (8), 3370−3377.

(4) García de Abajo, F. J. Graphene Plasmonics: Challenges and Opportunities. *ACS Photonics* **2014**, *1* (3), 135−152.

(5) Atwater, H. A.; Polman, A. Plasmonics for Improved Photovoltaic Devices. *Nat. Mater.* **2010**, *9* (3), 205−213.

(6) Jang, Y. H.; Jang, Y. J.; Kim, S.; Quan, L. N.; Chung, K.; Kim, D. H. Plasmonic Solar Cells: From Rational Design to Mechanism Overview. *Chem. Rev.* **2016**, *116* (24), 14982−15034.

(7) Yu, H.; Peng, Y.; Yang, Y.; Li, Z.-Y. Plasmon-Enhanced Light−Matter Interactions and Applications. *npj Comput. Mater.* **2019**, *5* (1), 45.

(8) Arinze, E. S.; Qiu, B.; Nyirjesy, G.; Thon, S. M. Plasmonic Nanoparticle Enhancement of Solution-Processed Solar Cells: Practical Limits and Opportunities. *ACS Photonics* **2016**, *3* (2), 158−173.

(9) Amirjani, A.; Amlashi, N. B.; Ahmadiani, Z. S. Plasmon-Enhanced Photocatalysis Based on Plasmonic Nanoparticles for Energy and Environmental Solutions: A Review. *ACS Appl. Nano Mater.* **2023**, *6* (11), 9085−9123.

(10) Ahlawat, M.; Mittal, D.; Govind Rao, V. Plasmon-Induced Hot-Hole Generation and Extraction at Nano-Heterointerfaces for Photocatalysis. *Commun. Mater.* **2021**, *2* (1), 114.

(11) Wang, X.; Huang, S.-C.; Hu, S.; Yan, S.; Ren, B. Fundamental Understanding and Applications of Plasmon-Enhanced Raman Spectroscopy. *Nat. Rev. Phys.* **2020**, *2* (5), 253−271.

(12) Su, Y.-H.; Ke, Y.-F.; Cai, S.-L.; Yao, Q.-Y. Surface Plasmon Resonance of Layer-by-Layer Gold Nanoparticles Induced Photoelectric Current in Environmentally-Friendly Plasmon-Sensitized Solar Cell. *Light:Sci. Appl.* **2012**, *1* (6), No. e14.

(13) Yadav, S.; Satija, J. The Current State of the Art of Plasmonic Nanofibrous Mats as SERS Substrates: Design, Fabrication and Sensor Applications. *J. Mater. Chem. B* **2021**, *9* (2), 267−282.

(14) Brown, A. M.; Sundararaman, R.; Narang, P.; Goddard, W. A.; Atwater, H. A. Nonradiative Plasmon Decay and Hot Carrier Dynamics: Effects of Phonons, Surfaces, and Geometry. *ACS Nano* **2016**, *10* (1), 957−966.

(15) Liau, Y.-H.; Unterreiner, A. N.; Chang, Q.; Scherer, N. F. Ultrafast Dephasing of Single Nanoparticles Studied by Two-Pulse Second-Order Interferometry. *J. Phys. Chem. B* **2001**, *105* (11), 2135−2142.

(16) Gieseking, R. L. M. P. Plasmons: untangling the classical, experimental, and quantum mechanical definitions. *Mater. Horiz.* **2022**, *9* (1), 25−42.

(17) Jeffries, W. R.; Park, K.; Vaia, R. A.; Knappenberger, K. L. Resolving Electron−Electron Scattering in Plasmonic Nanorod Ensembles Using Two-Dimensional Electronic Spectroscopy. *Nano Lett.* **2020**, *20* (10), 7722−7727.

(18) Link, S.; El-Sayed, M. A. Shape and Size Dependence of Radiative, Non-Radiative and Photothermal Properties of Gold Nanocrystals. *Int. Rev. Phys. Chem.* **2000**, *19* (3), 409−453.

(19) Chen, X.; Jensen, L. Understanding the Shape Effect on the Plasmonic Response of Small Ligand Coated Nanoparticles. *J. Opt.* **2016**, *18* (7), 074009.

(20) Gieseking, R. L.; Ratner, M. A.; Schatz, G. C. Semiempirical Modeling of Ag Nanoclusters: New Parameters for Optical Property Studies Enable Determination of Double Excitation Contributions to Plasmonic Excitation. *J. Phys. Chem. A* **2016**, *120* (26), 4542−4549.

(21) Herring, C. J.; Montemore, M. M. Recent Advances in Real-Time Time-Dependent Density Functional Theory Simulations of Plasmonic Nanostructures and Plasmonic Photocatalysis. *ACS Nanosci. Au* **2023**, *3* (4), 269−279.

(22) Zhou, M.; Higaki, T.; Hu, G.; Sfeir, M. Y.; Chen, Y.; Jiang, D.; Jin, R. Three-Orders-of-Magnitude Variation of Carrier Lifetimes with Crystal Phase of Gold Nanoclusters. *Science* **2019**, *364* (6437), 279−282.

(23) Kuda-Singappulige, G. U.; Aikens, C. M. Excited-State Absorption in Silver Nanoclusters. *J. Phys. Chem. C* **2021**, *125* (45), 24996−25006.

(24) Seveur, P.; Boubekeur-Lecaque, L.; Maurel, F.; Brémond, E.. Modeling the Photo-Absorption Properties of Noble Metal Nanoclusters: A Challenge for Density-Functional Theory. *J. Phys. Chem. C* **2023**, *127* (16), 7718−7729.

(25) Akola, J.; Walter, M.; Whetten, R. L.; Häkkinen, H.; Grönbeck, H. On the Structure of Thiolate-Protected Au_{25}. *J. Am. Chem. Soc.* **2008**, *130* (12), 3756−3757.

(26) Malola, S.; Lehtovaara, L.; Häkkinen, H. TDDFT Analysis of Optical Properties of Thiol Monolayer-Protected Gold and Intermetallic Silver−Gold $Au_{144}(SR)_{60}$ and $Au_{84}Ag_{60}(SR)_{60}$ Clusters. *J. Phys. Chem. C* **2014**, *118* (34), 20002−20008.

(27) Ding, F.; Guidez, E. B.; Aikens, C. M.; Li, X. Quantum Coherent Plasmon in Silver Nanowires: A Real-Time TDDFT Study. *J. Chem. Phys.* **2014**, *140* (24), 244705.

(28) Juarez-Mosqueda, R.; Malola, S.; Häkkinen, H. Stability, Electronic Structure, and Optical Properties of Protected Gold-Doped Silver $Ag_{29-x}Au_x$ (x = 0−5) Nanoclusters. *Phys. Chem. Chem. Phys.* **2017**, *19* (21), 13868−13874.

(29) Barcaro, G.; Sementa, L.; Fortunelli, A.; Stener, M. Optical Properties of Silver Nanoshells from Time-Dependent Density Functional Theory Calculations. *J. Phys. Chem. C* **2014**, *118* (23), 12450−12458.

(30) Aikens, C. M.; Li, S.; Schatz, G. C. From Discrete Electronic States to Plasmons: TDDFT Optical Absorption Properties of Ag_n (n = 10, 20, 35, 56, 84, 120) Tetrahedral Clusters. *J. Phys. Chem. C* **2008**, *112* (30), 11272−11279.
(31) Johnson, H. E.; Aikens, C. M. Electronic Structure and TDDFT Optical Absorption Spectra of Silver Nanorods. *J. Phys. Chem. A* **2009**, *113* (16), 4445−4450.
(32) Dillon, A. D.; Gieseking, R. L. M. Evolution of Plasmon-like Excited States in Silver Nanowires and Nanorods. *J. Chem. Phys.* **2022**, *156* (7), 074301.
(33) Tussupbayev, S.; Govind, N.; Lopata, K.; Cramer, C. J. Comparison of Real-Time and Linear-Response Time-Dependent Density Functional Theories for Molecular Chromophores Ranging from Sparse to High Densities of States. *J. Chem. Theory Comput.* **2015**, *11* (3), 1102−1109.
(34) Li, X.; Smith, S. M.; Markevitch, A. N.; Romanov, D. A.; Levis, R. J.; Schlegel, H. B. A Time-Dependent Hartree−Fock Approach for Studying the Electronic Optical Response of Molecules in Intense Fields. *Phys. Chem. Chem. Phys.* **2005**, *7* (2), 233−239.
(35) Takimoto, Y.; Vila, F. D.; Rehr, J. J. Real-Time Time-Dependent Density Functional Theory Approach for Frequency-Dependent Nonlinear Optical Response in Photonic Molecules. *J. Chem. Phys.* **2007**, *127* (15), 154114.
(36) Meng, S.; Kaxiras, E. Real-Time, Local Basis-Set Implementation of Time-Dependent Density Functional Theory for Excited State Dynamics Simulations. *J. Chem. Phys.* **2008**, *129* (5), 054110.
(37) Trepl, T.; Schelter, I.; Kümmel, S. Analyzing Excitation-Energy Transfer Based on the Time-Dependent Density Functional Theory in Real Time. *J. Chem. Theory Comput.* **2022**, *18* (11), 6577−6587.
(38) Provorse, M. R.; Habenicht, B. F.; Isborn, C. M. Peak-Shifting in Real-Time Time-Dependent Density Functional Theory. *J. Chem. Theory Comput.* **2015**, *11* (10), 4791−4802.
(39) Madison, L. R.; Ratner, M. A.; Schatz, G. C. Understanding the Electronic Structure Properties of Bare Silver Clusters as Models for Plasmonic Excitation. *Frontiers in Quantum Methods and Applications in Chemistry and Physics*; Springer: Cham, 2015; pp 37−52..
(40) Conley, K. M.; Nayyar, N.; Rossi, T. P.; Kuisma, M.; Turkowski, V.; Puska, M. J.; Rahman, T. S. Plasmon Excitations in Mixed Metallic Nanoarrays. *ACS Nano* **2019**, *13* (5), 5344−5355.
(41) Hauge, E.; Kristiansen, H. E.; Konecny, L.; Kadek, M.; Repisky, M.; Pedersen, T. B. Cost-Efficient High-Resolution Linear Absorption Spectra through Extrapolating the Dipole Moment from Real-Time Time-Dependent Electronic-Structure Theory. *J. Chem. Theory Comput.* **2023**, *19* (21), 7764−7775.
(42) Sinha-Roy, R.; García-González, P.; López Lozano, X.; Whetten, R. L.; Weissker, H.-C. Identifying Electronic Modes by Fourier Transform from δ-Kick Time-Evolution TDDFT Calculations. *J. Chem. Theory Comput.* **2018**, *14* (12), 6417−6426.
(43) Rossi, T. P.; Kuisma, M.; Puska, M. J.; Nieminen, R. M.; Erhart, P. Kohn−Sham Decomposition in Real-Time Time-Dependent Density-Functional Theory: An Efficient Tool for Analyzing Plasmonic Excitations. *J. Chem. Theory Comput.* **2017**, *13* (10), 4779−4790.
(44) Yan, J.; Gao, S. Plasmon Resonances in Linear Atomic Chains: Free-Electron Behavior and Anisotropic Screening of Electrons. *Phys. Rev. B:Condens. Matter Mater. Phys.* **2008**, *78* (23), 235413.
(45) Gao, B.; Ruud, K.; Luo, Y. Plasmon Resonances in Linear Noble-Metal Chains. *J. Chem. Phys.* **2012**, *137* (19), 194307.
(46) Kuda-Singappulige, G. U.; Lingerfelt, D. B.; Li, X.; Aikens, C. M. Ultrafast Nonlinear Plasmon Decay Processes in Silver Nanoclusters. *J. Phys. Chem. C* **2020**, *124* (37), 20477−20487.
(47) Ma, J.; Wang, Z.; Wang, L.-W. Interplay between Plasmon and Single-Particle Excitations in a Metal Nanocluster. *Nat. Commun.* **2015**, *6* (1), 10107.
(48) Chapman, C. T.; Liang, W.; Li, X. Ultrafast Coherent Electron−Hole Separation Dynamics in a Fullerene Derivative. *J. Phys. Chem. Lett.* **2011**, *2* (10), 1189−1192.
(49) Kuda-Singappulige, G. U.; Wildman, A.; Lingerfelt, D. B.; Li, X.; Aikens, C. M. Ultrafast Nonradiative Decay of a Dipolar Plasmon-like State in Naphthalene. *J. Phys. Chem. A* **2020**, *124* (47), 9729−9737.
(50) Repisky, M.; Konecny, L.; Kadek, M.; Komorovsky, S.; Malkin, O. L.; Malkin, V. G.; Ruud, K. Excitation Energies from Real-Time Propagation of the Four-Component Dirac−Kohn−Sham Equation. *J. Chem. Theory Comput.* **2015**, *11* (3), 980−991.
(51) Neese, F. Prediction of Molecular Properties and Molecular Spectroscopy with Density Functional Theory: From Fundamental Theory to Exchange-Coupling. *Coord. Chem. Rev.* **2009**, *253* (5−6), 526−563.
(52) Rowe, D. J. An Intepretation of Time-Dependent Hartree-Fock Theory. *Nucl. Phys.* **1966**, *80* (1), 209−222.
(53) Peterson, K. A.; Puzzarini, C. Systematically Convergent Basis Sets for Transition Metals. II. Pseudopotential-Based Correlation Consistent Basis Sets for the Group 11 (Cu, Ag, Au) and 12 (Zn, Cd, Hg) Elements. *Theor. Chem. Acc.* **2005**, *114* (4−5), 283−296.
(54) Adamo, C.; Barone, V. Toward Reliable Density Functional Methods without Adjustable Parameters: The PBE0Model. *J. Chem. Phys.* **1999**, *110* (13), 6158−6170.
(55) Casida, M. E.; Casida, K. C.; Salahub, D. R. Excited-State Potential Energy Curves from Time-Dependent Density-Functional Theory: A Cross Section of Formaldehyde's1A1Manifold. *Int. J. Quantum Chem.* **1998**, *70* (4−5), 933−941.
(56) Lopata, K.; Govind, N. Modeling Fast Electron Dynamics with Real-Time Time-Dependent Density Functional Theory: Application to Small Molecules and Chromophores. *J. Chem. Theory Comput.* **2011**, *7* (5), 1344−1355.
(57) Casida, M. E.; Jamorski, C.; Casida, K. C.; Salahub, D. R. Molecular Excitation Energies to High-Lying Bound States from Time-Dependent Density-Functional Response Theory: Characterization and Correction of the Time-Dependent Local Density Approximation Ionization Threshold. *J. Chem. Phys.* **1998**, *108* (11), 4439−4449.
(58) Mullin, J. M.; Autschbach, J.; Schatz, G. C. Time-Dependent Density Functional Methods for Surface Enhanced Raman Scattering (SERS) Studies. *Comput. Theor. Chem.* **2012**, *987*, 32−41.
(59) Aprà, E.; Bylaska, E. J.; de Jong, W. A.; Govind, N.; Kowalski, K.; Straatsma, T. P.; Valiev, M.; van Dam, H. J. J.; Alexeev, Y.; Anchell, J.; Anisimov, V.; Aquino, F. W.; Atta-Fynn, R.; Autschbach, J.; Bauman, N. P.; Becca, J. C.; Bernholdt, D. E.; Bhaskaran-Nair, K.; Bogatko, S.; Borowski, P.; Boschen, J.; Brabec, J.; Bruner, A.; Cauët, E.; Chen, Y.; Chuev, G. N.; Cramer, C. J.; Daily, J.; Deegan, M. J. O.; Dunning, T. H.; Dupuis, M.; Dyall, K. G.; Fann, G. I.; Fischer, S. A.; Fonari, A.; Früchtl, H.; Gagliardi, L.; Garza, J.; Gawande, N.; Ghosh, S.; Glaesemann, K.; Götz, A. W.; Hammond, J.; Helms, V.; Hermes, E. D.; Hirao, K.; Hirata, S.; Jacquelin, M.; Jensen, L.; Johnson, B. G.; Jónsson, H.; Kendall, R. A.; Klemm, M.; Kobayashi, R.; Konkov, V.; Krishnamoorthy, S.; Krishnan, M.; Lin, Z.; Lins, R. D.; Littlefield, R. J.; Logsdail, A. J.; Lopata, K.; Ma, W.; Marenich, A. V.; Martin del Campo, J.; Mejia-Rodriguez, D.; Moore, J. E.; Mullin, J. M.; Nakajima, T.; Nascimento, D. R.; Nichols, J. A.; Nichols, P. J.; Nieplocha, J.; Otero-de-la-Roza, A.; Palmer, B.; Panyala, A.; Pirojsirikul, T.; Peng, B.; Peverati, R.; Pittner, J.; Pollack, L.; Richard, R. M.; Sadayappan, P.; Schatz, G. C.; Shelton, W. A.; Silverstein, D. W.; Smith, D. M. A.; Soares, T. A.; Song, D.; Swart, M.; Taylor, H. L.; Thomas, G. S.; Tipparaju, V.; Truhlar, D. G.; Tsemekhman, K.; Van Voorhis, T.; Vázquez-Mayagoitia, Á.; Verma, P.; Villa, O.; Vishnu, A.; Vogiatzis, K. D.; Wang, D.; Weare, J. H.; Williamson, M. J.; Windus, T. L.; Woliński, K.; Wong, A. T.; Wu, Q.; Yang, C.; Yu, Q.; Zacharias, M.; Zhang, Z.; Zhao, Y.; Harrison, R. J. NWChem: Past, Present, and Future. *J. Chem. Phys.* **2020**, *152* (18), 184102.
(60) Ilawe, N. V.; Oviedo, M. B.; Wong, B. M. Real-Time Quantum Dynamics of Long-Range Electronic Excitation Transfer in Plasmonic Nanoantennas. *J. Chem. Theory Comput.* **2017**, *13* (8), 3442−3454.
(61) Weerawardene, K. L. D. M.; Aikens, C. M. Comparison and Convergence of Optical Absorption Spectra of Noble Metal Nanoparticles Computed Using Linear-Response and Real-Time Time-Dependent Density Functional Theories. *Comput. Theor. Chem.* **2018**, *1146*, 27−36.

https://doi.org/10.1021/acs.jctc.4c01302
J. Chem. Theory Comput. 2025, 21, 17−28

(62) Yan, J.; Yuan, Z.; Gao, S. End and Central Plasmon Resonances in Linear Atomic Chains. *Phys. Rev. Lett.* **2007**, *98* (21), 216602.
(63) Peng, B.; Lingerfelt, D. B.; Ding, F.; Aikens, C. M.; Li, X. Real-Time TDDFT Studies of Exciton Decay and Transfer in Silver Nanowire Arrays. *J. Phys. Chem. C* **2015**, *119* (11), 6421−6427.
(64) Karimova, N. V.; Aikens, C. M. Time-Dependent Density Functional Theory Investigation of the Electronic Structure and Chiroptical Properties of Curved and Helical Silver Nanowires. *J. Phys. Chem. A* **2015**, *119* (29), 8163−8173.
(65) Guidez, E. B.; Aikens, C. M. Theoretical Analysis of the Optical Excitation Spectra of Silver and Gold Nanowires. *Nanoscale* **2012**, *4* (14), 4190.

https://doi.org/10.1021/acs.jctc.4c01302
J. Chem. Theory Comput. 2025, 21, 17−28